Lecture note Magnetism (9)

8th June (2022) Shingo Katsumoto, Institute for Solid State Physics, University of Tokyo

In the last lecture, we stopped at the molecular field approximation of anti-ferromagnetic Heisenberg model. The lecture note was at the beginning of ferrimagnetism. I would like to add the treatment of parallel magnetic field to spontaneous (internal) magnetization of an anti-ferromagnetic state. And would like to change some notations in the ferrimagnetic part. Hence, here, I would like to rewrite the ferrimagnetic part.

5.5.1 Parallel susceptibility

Next we consider the case that the external magnetic field is parallel or anti-parallel (collinear) to the spontaneous magnetizations of sublattices. The Heisenberg model is completely isotropic. If we assume that the system always takes the lowest energy state, then the magnetization should rotate to be perpendicular to the external magnetic field. However real materials usually have some magnetic anisotropies that lock the directions of moment. We thus consider the case the external field is collinear to the spontaneous magnetization. The effective fields in A and B sublattices are written as

$$B_{\mathrm{eff}}(\mathrm{A}) = B + B_{\mathrm{sub}}(\mathrm{A}), \tag{5.37a}$$
$$B_{\mathrm{eff}}(\mathrm{B}) = B + B_{\mathrm{sub}}(\mathrm{B}). \tag{5.37b}$$

Because the vectors are collinear, we do not use vector symbols here. Then as is due course, we write down a set of self-consistent equations for magnetizations as

$$\begin{aligned} \langle M_{\mathrm{A}} \rangle &= \mu S \mathcal{B}_S \left[\frac{\mu S}{k_{\mathrm{B}} T} \left(B + \frac{2\alpha_z J}{\mu^2} \langle M_{\mathrm{B}} \rangle \right) \right], \\ \langle M_{\mathrm{B}} \rangle &= \mu S \mathcal{B}_S \left[\frac{\mu S}{k_{\mathrm{B}} T} \left(B + \frac{2\alpha_z J}{\mu^2} \langle M_{\mathrm{A}} \rangle \right) \right], \end{aligned} \tag{5.38}$$

where $\mathcal{B}_S(x)$ is the Brillouin function. With solving the above and from the relation [*1] ,

$$\chi_{\parallel} = \lim_{B \to 0} \frac{M_A + M_B}{B}, \tag{5.39}$$

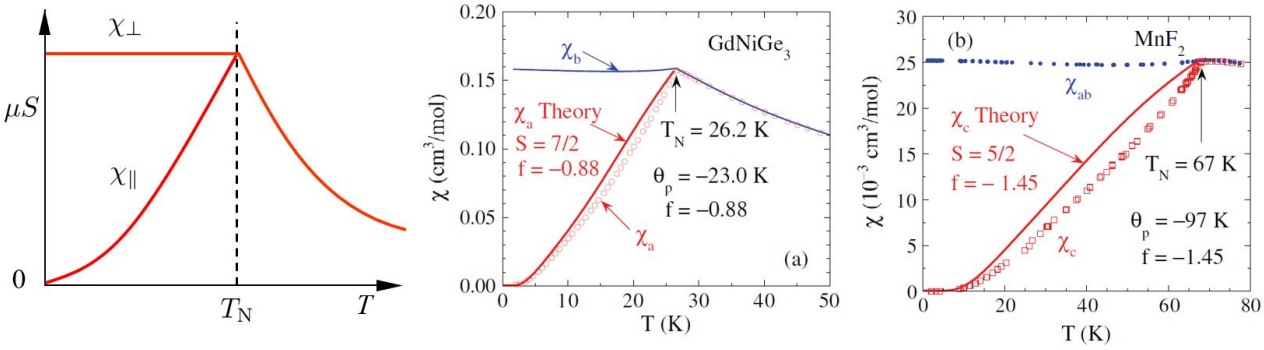

Fig. 5.1 Left panel: Schematic diagram of temperature dependent susceptibility in the molecular field approximation of the anti-ferromagnetic Heisenberg model. The susceptibilities for magnetic field perpendicular ($\chi_\perp$) and parallel ($\chi_\parallel$) to the spin polarization. Measured susceptibilities of (a) $GdNiGe_3$, (b) MnF_2. From [1].

[*1] As is the case of spontaneous ferromagnetic magnetization, we need to solve the equation numerically.

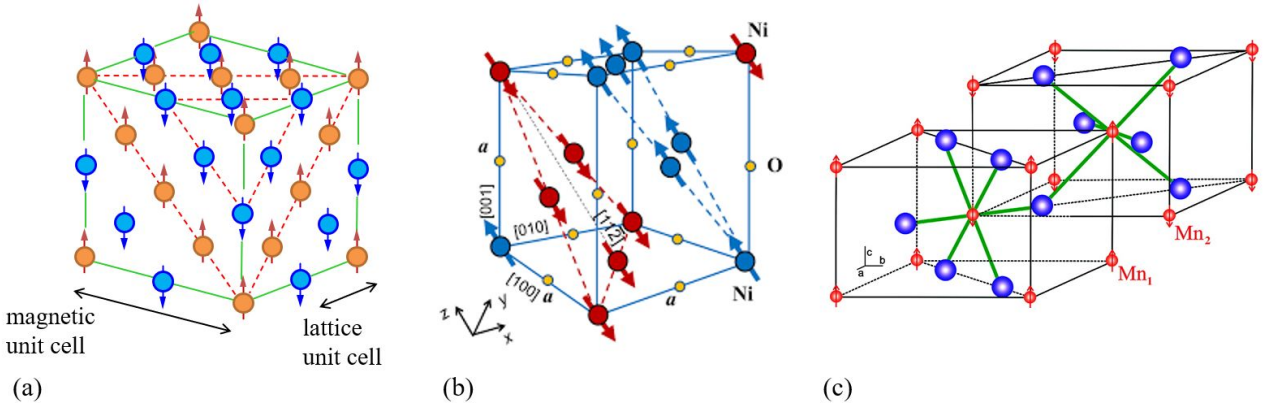

Fig. 5.2 Examples of spin configurations in metal oxides, fluorides. (a) and (b) shows the spin-directions at magnetic ions. (c) also shows the positions of F-atoms. (a) MnO. From [2]. Red broken lines show the sheets of aligned spins. (b) NiO. From [3]. (c) MnF_2. From [4].

we obtain the parallel magnetization.

From eq. (5.38), in the limit of $T \to 0$, $M_{\rm A} = -M_{\rm B} = \mu S$ as in the case of ferromagnetism, $\chi_\parallel \to 0$. On the other hand, $\chi_\parallel = \chi_\perp$ at $T = T_{\rm N}$ The susceptibility, thus has a large anisotropy below $T_{\rm N}$ as shown in the left panel of Fig. 5.1. Though the situation of perpendicular field to the sublattice magnetization cannot be realized in the Heisenberg model, a small anisotropy may enable it. In many anti-ferromagnets, such properties have been really observed. Figure 5.1(a), (b) show examples of $GdNiGe_3$, MnF_2, which are claimed to be close to the anti-ferromagnetic Heisenberg model.

5.5.2 Antiferromagnetic insulators

So far, we have discussed the magnetic susceptibility of antiferromagnetic materials with a very simple two-dimensional Heisenberg model. As mentioned in the section on superexchange interactions, oxides and fluorides of magnetic metals are often antiferromagnetic. Figure 5.2 shows examples of spin configurations in anti-ferromagnetic insulators. As in the Heisenberg model, neighboring (though with intermediate negative ions) spins at magnetic ions have opposite directions. As can be seen in the figure, actual "sublattices" can be taken as two-dimensional spin-aligned sheets. In such a case, the structure is a kind of magnetic superlattice.

In an anti-ferromagnetic ordered state, the spins have a periodic structure with a larger volume than that of lattice (unit cell). This is sometimes called a spin-superlattice. For this situation, we can apply a concept called **magnetic unit cell**, which is the unit of periodicity including the spin configuration. These two kinds of unit cell lengths are indicated in Fig. 5.2(a).

$\chi_{\rm u}$ in eq. (5.31a) does not diverge because $J < 0$. Instead it shows the temperature dependence

$$\chi_{\rm u} \propto \frac{1}{T+\theta}, \tag{5.40}$$

which is different from the Curie law. This θ is called **Weiss temperature**.

The Néel temperatures and the Weiss temperatures of typical anti-ferromagnets are liste in Tab. 5.1. From eqs. (5.31,32), these two kinds of temperatures should be symmetric to 0 K. Of course, a simple model even without anisotropy should give results far different from the reality. However, there is some rough correlation between them.

Material	Lattice-type of magnetic ions	Néel temperature (K)	Weiss temperature (K)
MnO	fcc	116	610
MnS	fcc	160	528
MnTe	hexagonal	307	690
MnF_2	bct	67	82
FeF_2	bct	79	117
$FeCl_2$	hexagonal	24	48
FeO	fcc	198	570
$CoCl_2$	hexagonal	25	38
CoO	fcc	291	330
$NiCl_2$	hexagonal	50	62
NiO	fcc	525	~ 2000
Cr	fcc	308	

Tab. 5.1 Néel temperatures and Weiss temperatures of typical anti-ferromagnets.

5.5.3 Spin flop transition and metamagnetism

Consider a general material with susceptibility χ. With increasing the external magnetic field, the energy gain due to the magnetization is

$$E_{\mathrm{m}} = -\int_0^B \frac{M(B')}{\mu_0}\frac{dB'}{\mu_0} = -\chi\int_0^B \frac{B'}{\mu_0}\frac{dB'}{\mu_0} = -\frac{\chi}{2\mu_0^2}B^2. \tag{5.41}$$

In the region $T < T_{\mathrm{N}}$, $\chi_\perp > \chi_\parallel$ as shown in Fig. 5.1, hence the energy is lower for the magnetic field perpendicular to the sublattice magnetization. As mentioned in the beginning of "parallel susceptibility," with increasing a parallel field, the energy difference overcomes the anisotropic energy K at a certain point, at which the sublattice magnetizations rotate to the direction perpendicular to the magnetic field. This is called **spin flop transition**. The critical field is obtained from

$$\frac{\chi_\perp - \chi_\parallel}{2\mu_0^2}B_{\mathrm{c}}^2 = K, \tag{5.42}$$

as

$$B_{\mathrm{c}} = \mu_0\sqrt{\frac{2K}{\chi_\perp - \chi_\parallel}}. \tag{5.43}$$

After the transition, the field also gives an oblique angle to sublattice magnetizations as shown in Fig. 5.3(a). In the process of increasing field, the total magnetization increases with the field proportionally and saturates at the field of complete polarization.

In conventional anti-ferromagnets, this critical field is too large to reach in many of laboratories. Recently, however, there have been many reports on the spin flop transition in nano-ferromagnets or in molecular ferromagnets. Figure 5.3(b) shows such an example of a crystal composed of a polymer $\{[\mathrm{Mn_2(bpdo)(H_2O)_4}][\mathrm{Nb(CN)_8}]\cdot 6\mathrm{H_2O}\}_n$. It has Néel point at T_{N}=15 K, which is comparatively low. We observe a clear spin flop transition at around 0.6 T at 1.8 K.

So far we have considered the case of nearest-neighbor-only exchange interaction. That is, only inter-sublattice interaction is considered and intra-sublattice interaction is ignored. In reality, the super-exchange interaction often works between spins in a sublattice (intra-sublattice interaction). In some cases, an anti-ferromagnetism at zero field is realized by a small difference in inter-sublattice anti-ferromagnetic interaction and intra-sublattice ferromagnetic interaction. In such a case, increasing the external field lowers the energy of magnetic moments parallel to the field. And at a certain

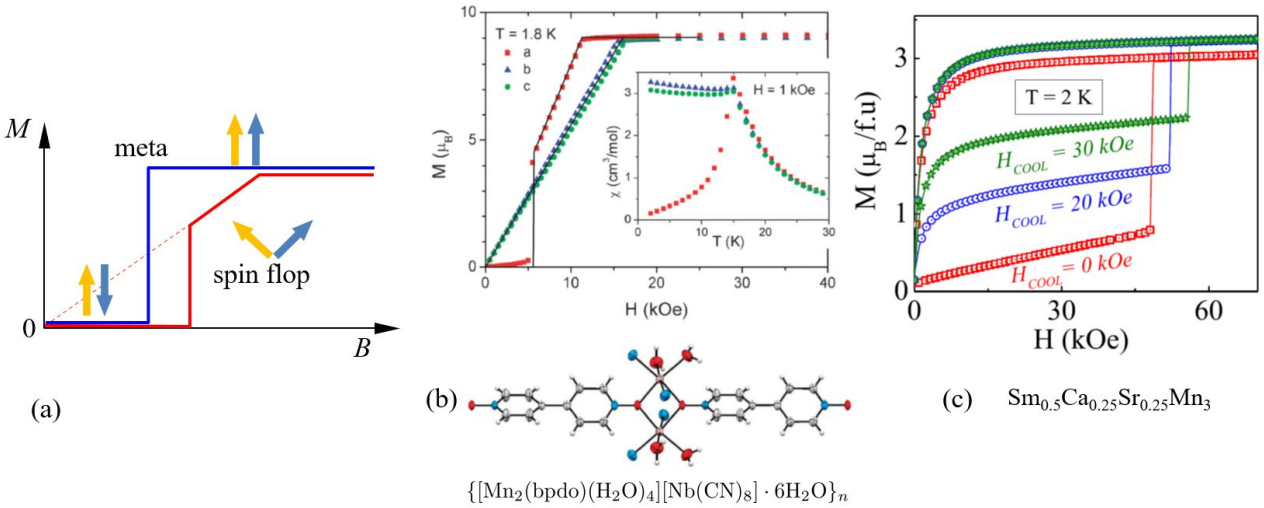

Fig. 5.3 (a) Illustration of spin flop transition (red line) and metamagnetism (blue line). (b) Spin flop transition appeared in a polymer anti-ferromagnet $\{[Mn_2(bpdo)(H_2O)_4][Nb(CN)_8]\cdot 6H_2O\}_n$. The inset shows the susceptibility at a low (0.1 T) field. It is an anti-ferromagnet with T_N=15 K, with the spin-easy axis along a-axis. From [5]. Lower panel shows the molecular structure with axes b (pointing up), c (pointing left), a (coming up from this paper). (c) Examples of metamagnetic transition in a Mott insulator $Sm_{0.5}Ca_{0.25}Sr_{0.25}MnO_3$[6].

field, the whole system goes to a ferromagnetic, which phenomenon appears as a sudden or steep increase in magnetization up to the saturation. This is called **meta-magnetism**[6]. An example is shown in Fig. 5.3(c). Meta-magnetism often has strong temperature dependence. If we fix the magnetic field close to the critical field, the temperature also drives a meta magnetic transition, which gives a very large $(\partial M/\partial T)_B$. From eq. (2.114), this is very advantageous for magnetic refrigeration. And now the application of meta-magnetism to high-efficiency magnetic refrigeration is active([7] is an example from a helimagnetism).

5.6 Ferrimagnetism

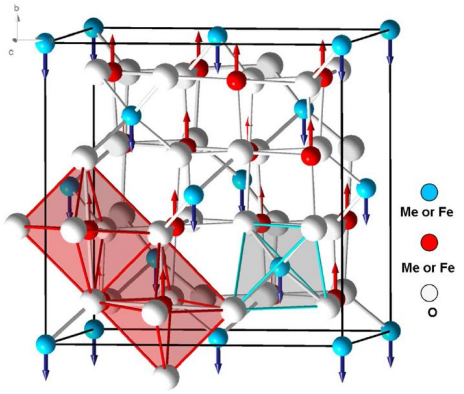

The most typical material of magnetic insulators is ferrite, which I mentioned in the beginning of this chapter.

5.6.1 Magnetism in ferrite

In the ferromagnetism of ferrite (AFe_2O_4, A=Mn, Co, Ni, Cu, Zn, $\cdots$), the spin-alignment is a mixture of anti-ferro and ferro types. Because the sublattices have different magnetic moments, they do not cancel out. As a result a total finite spontaneous magnetization appears. Such magnetism is named **ferrimagnetism** after ferrite.

In the unit cell of spinel-type ferrite, there are 16 Fe^{3+}, 8 M^{2+}, 32 O^{2-}. Spin magnetic moments at Fe ions are mostly cancelled by anti-ferromagnetic interaction, and spins at M^{2+} survive, causing the ferrimagnetism. The expected magnetic moments of ferrite and experimental values along with this statement are listed below showing a good agreement.

Materials	$MnFe_2O_4$	$FeFe_2O_4$	$CoFe_2O_4$	$NiFe_2O_4$	$CuFe_2O_4$
Moment (Theory)	$5\mu_B$	$4\mu_B$	$3\mu_B$	$2\mu_B$	$1\mu_B$
Moment (Exp.)	5.0	4.2	3.3	2.3	1.3
T_N (K)	783	848	793	863	728

A bit detailed discussions on the magnetism of ferrite can be found in ref. [8] (in Japanese), or in refs. [9, 10]. For the application of ferrite magnetism, refer to refs. [11, 12]. Ferrite is extremely important in industrial application. They show various magnetism depending on species of M, crystal types and shapes of samples. Even now, research is extremely active, and many review papers for each individual ferrite can be found even in the last few years.

5.6.2 Molecular field approximation of ferrimagnetism

We here use a Heisenberg model with unbalanced sublattices A and B.

$$B_A = \alpha M_A + (-\gamma)(-M_B) = \alpha M_A + \gamma M_B, \tag{5.44a}$$
$$B_B = \gamma M_A + \beta M_B, \tag{5.44b}$$

where we consider not only inter-sublattice exchange interaction but also intra-sublattice interaction. The imbalance is taken into account by the difference between α, β. The inter-sublattice interaction is γ (must be common).

5.6.3 Magnetization below the Néel temperature

The set of self-consistent equations for magnetizations M_A and M_B in sublattices is from molecular field approximation (5.44) as

$$M_A = \mu S_A \mathcal{B}_{S_A}\left[\frac{\mu S_A}{k_B T}(\alpha M_A + \gamma M_B)\right], \tag{5.45a}$$
$$M_B = \mu S_B \mathcal{B}_{S_B}\left[\frac{\mu S_B}{k_B T}(\gamma M_A + \beta M_B)\right], \tag{5.45b}$$

where the Brillouin function is written as $\mathcal{B}_S(x)$. Though $\mu = g\mu_B$ may be different for sublattices if g-factors are different, we here assume they are common for simplicity.

To obtain M_A, M_B, thus the total magnetization $M = M_A - M_B$, we need to solve eq. (5.45) numerically.

In such compensated ferrimagnetism, magnetizations show complicated temperature dependences below Néel temperature due to the differences between S_A and S_B, α and β. As an example, compensated ferrimagnetism is displayed in

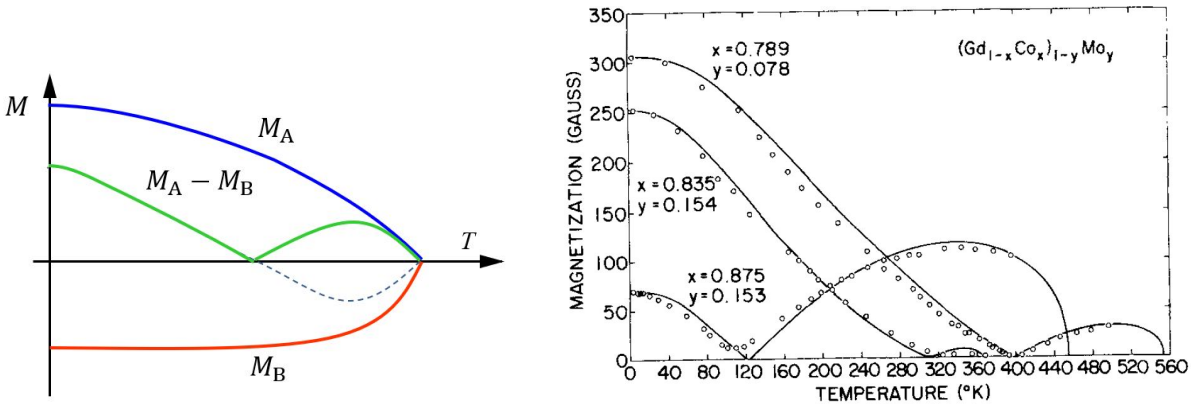

(a) (b)

Fig. 5.4 (a) Conceptual scheme of compensated ferrimagnetism. (b) Compensated ferrimagnetism appeared in the magnetization of amorphous alloy Gd-Co-Mn. From [13].

Fig. 5.4. In conceptual diagram in Fig. 5.4(a), A-sublattice has a larger lowest temperature magnetization ($S_{\mathrm{A}} > S_{\mathrm{B}}$). On the other hand, B-sublattice has a larger intra-sublattice interaction ($\beta < \alpha$), then the growth of magnetization M_{B} below Néel is faster with lowering the temperature. Hence in a certain temperature region lower than T_{N}, $M_{\mathrm{B}} > M_{\mathrm{A}}$ holds and as indicated by the broken line $M_{\mathrm{A}} - M_{\mathrm{B}}$ is negative though in the measurement, magnetization M parallel to the field always has lower energy and the green line is observed. With lowering of temperature, M_{A} increases and the total magnetization disappears at the point of $M_{\mathrm{A}} = M_{\mathrm{B}}$. But with further lowering of temperature, $M_{\mathrm{A}} > M_{\mathrm{B}}$ and the magnetization reappears. As a whole, it becomes a curious temperature dependence as shown by the green line. Figure 5.4(b) shows such a temperature dependence of an amorphous alloy Gd-Co-Mo[13]. In "complete compensation type" ferrimagnetism, there is a difference in intra-interaction but the sublattice magnetic moments are the same and the total magnetization disappears at lowest temperatures[14].

5.7 Helimagnetism

It is not alway possible to separate a spin system with anti-ferromagnetic interaction into a small numbers of magnetic sublattices. Also as considered in the previous section, ranges of interactions may span over more than single (magnetic) lattice constant. Let us consider **helimagnetism**, that appears in such a complex system in a Heisenberg model. It has a spiral-like spin configuration, which shows considerable difference from parallel/anti-parallel (collinear) configurations so far considered. In the treatment of anti-ferromagnetism, firstly the anti-ferromagnetic ground state (Néel ordered state) is given. Then the molecular field is considered based on the state. This time, we have a look on the process to find out the ground state[15].

5.7.1 Classical Heisenberg model

Here the exchange interaction potential J depends on the combination of sites (i, j) and a site-dependent magnetic field $\boldsymbol{B}_i$ is working on each site.

$$\mathscr{H} = -\sum_{\langle i,j \rangle} J_{ij} \boldsymbol{S}_i \cdot \boldsymbol{S}_j - \mu \sum_i \boldsymbol{B}_i \cdot \boldsymbol{S}_i. \tag{5.46}$$

However we put $\boldsymbol{B}_i = \boldsymbol{0}$ for a while. And in the first place, to see that a helical spin configuration can be stable, we consider a classical Heisenberg model, in that the spins are treated as classical vectors.

To look for an ordered stated, we assume an ordered state and perform Fourier expansion as

$$\langle \boldsymbol{S}_i \rangle = \frac{1}{\sqrt{N}} \sum_{\boldsymbol{q}} \langle \boldsymbol{S}_{\boldsymbol{q}} \rangle \exp(i\boldsymbol{q} \cdot \boldsymbol{r}_i). \tag{5.47}$$

Then

$$|\langle \boldsymbol{S}_i \rangle|^2 = S^2 = \frac{1}{N} \sum_{\boldsymbol{q},\boldsymbol{q}'} \langle \boldsymbol{S}_{\boldsymbol{q}} \rangle \cdot \langle \boldsymbol{S}_{\boldsymbol{q}'} \rangle \exp(i(\boldsymbol{q} + \boldsymbol{q}') \cdot \boldsymbol{r}_i) \tag{5.48}$$

Now the expectation value of Hamiltonian can be written as

$$\langle \mathscr{H} \rangle = -\sum_{\langle i,j \rangle} J_{ij} \langle \boldsymbol{S}_i \rangle \cdot \langle \boldsymbol{S}_j \rangle = -\sum_{\boldsymbol{q}} J_{\boldsymbol{q}} \langle \boldsymbol{S}_{\boldsymbol{q}} \rangle \cdot \langle \boldsymbol{S}_{-\boldsymbol{q}} \rangle, \tag{5.49}$$

where

$$J_{\boldsymbol{q}} = \sum_j J_{ij} \exp[-i\boldsymbol{q} \cdot (\boldsymbol{r}_i - \boldsymbol{r}_j)] \tag{5.50}$$

is the Fourier transform of the interaction potential. Taking the sum of both sides of eq. (5.48)on subscript i, the right hand side is

$$\frac{1}{N} \sum_i \sum_{\boldsymbol{q},\boldsymbol{q}'} \langle \boldsymbol{S}_{\boldsymbol{q}} \rangle \cdot \langle \boldsymbol{S}_{\boldsymbol{q}'} \rangle \exp(i(\boldsymbol{q} + \boldsymbol{q}') \cdot \boldsymbol{r}_i) = \sum_{\boldsymbol{q},\boldsymbol{q}'} \langle \boldsymbol{S}_{\boldsymbol{q}} \rangle \cdot \langle \boldsymbol{S}_{\boldsymbol{q}'} \rangle \delta_{\boldsymbol{q},-\boldsymbol{q}'}.$$

Then

$$NS^2 = \sum_{\boldsymbol{q}} \langle \boldsymbol{S}_{\boldsymbol{q}} \rangle \cdot \langle \boldsymbol{S}_{-\boldsymbol{q}} \rangle \,. \tag{5.51}$$

This works as a condition fulfilled by the classical solution.

In the Heisenberg model, $J_{ij} = J_{ji}$ and also is real, $J_{\boldsymbol{q}}$ should be an even function of $\boldsymbol{q}$. We then assume that $J_{\boldsymbol{q}}$ takes the maximum (i.e., has a repeating structure with a finite period), and let $\pm\boldsymbol{Q}$ be the wavenubers that give the maxima to $J_{\boldsymbol{q}}$. When $\boldsymbol{Q} = \boldsymbol{K} - \boldsymbol{Q}$ with an inverse lattice vector $\boldsymbol{K}$, the system is in classical anti-ferromagnetic state, and out of our scope here. Then though it is a bit bold, under the condition (5.51), we assume

$$\langle \boldsymbol{S}_{\boldsymbol{Q}} \rangle \neq 0, \quad \langle \boldsymbol{S}_{-\boldsymbol{Q}} \rangle \neq 0, \quad (\text{others}) = 0. \tag{5.52}$$

Then eq. (5.48) can be written as follows:

$$NS^2 = \langle \boldsymbol{S}_{\boldsymbol{Q}} \rangle \cdot \langle \boldsymbol{S}_{\boldsymbol{Q}} \rangle \exp(2i\boldsymbol{Q} \cdot \boldsymbol{r}_i) + \langle \boldsymbol{S}_{-\boldsymbol{Q}} \rangle \cdot \langle \boldsymbol{S}_{-\boldsymbol{Q}} \rangle \exp(-2i\boldsymbol{Q} \cdot \boldsymbol{r}_i) + 2 \langle \boldsymbol{S}_{\boldsymbol{Q}} \rangle \cdot \langle \boldsymbol{S}_{-\boldsymbol{Q}} \rangle \,. \tag{5.53}$$

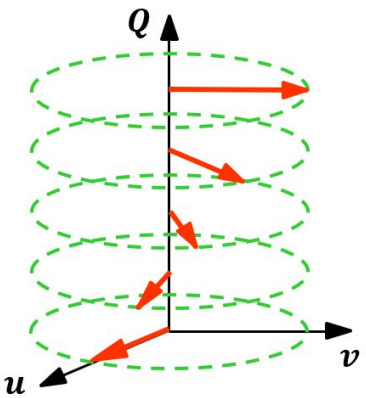

Because the sum in the rhs of eq. (5.51) should be taken for $\boldsymbol{q} = \pm\boldsymbol{Q}$, in the present case $2 \langle \boldsymbol{S}_{\boldsymbol{Q}} \rangle \cdot \langle \boldsymbol{S}_{-\boldsymbol{Q}} \rangle$, that just corresponds to the third term in eq. (5.53). From the above we get

$$\langle \boldsymbol{S}_{\boldsymbol{Q}} \rangle \cdot \langle \boldsymbol{S}_{\boldsymbol{Q}} \rangle = \langle \boldsymbol{S}_{-\boldsymbol{Q}} \rangle \cdot \langle \boldsymbol{S}_{-\boldsymbol{Q}} \rangle = 0. \tag{5.54}$$

This condition is, for example, for $\langle \boldsymbol{S}_{\boldsymbol{Q}} \rangle$,

$$\mathrm{Re}[\langle \boldsymbol{S}_{\boldsymbol{Q}} \rangle] = \boldsymbol{a}, \ \mathrm{Im}[\langle \boldsymbol{S}_{\boldsymbol{Q}} \rangle] = \boldsymbol{b} \longmapsto |\boldsymbol{a}|^2 - |\boldsymbol{b}|^2 = 0, \ \boldsymbol{a} \cdot \boldsymbol{b} = 0, \tag{5.55}$$

that is, the amplitude of the real and the imaginary parts are the same and they should be orthogonal. Then, we can write

$$\langle \boldsymbol{S}_{\boldsymbol{Q}} \rangle = \frac{\sqrt{N}}{2} S(\boldsymbol{u} - i\boldsymbol{v}), \tag{5.56}$$

where $\boldsymbol{u}$ and $\boldsymbol{v}$ are orthogonal unit vectors. This leads to the expectation value of spins in the ground state:

$$\langle \boldsymbol{S}_i \rangle = S[\boldsymbol{u} \cos(\boldsymbol{Q} \cdot \boldsymbol{r}_i) + \boldsymbol{v} \sin(\boldsymbol{Q} \cdot \boldsymbol{r}_i)]. \tag{5.57}$$

In this spin configuration, the spin rotates along and around $\boldsymbol{Q}$-axis in the plane stretched by $(\boldsymbol{u} and \boldsymbol{v})$. The configuration is called **helical spin structure**. Though the structure is affected by crystal anisotropy in real materials, the theoretical Heisenberg model is isotropic and the plane of $(\boldsymbol{u}, \boldsymbol{v})$ can be taken to any direction.

5.7.2 Molecular field approximation

Based on the classical ground state, we apply the molecular field approximation, by introducing the site-dependent magnetic field

$$\boldsymbol{B}_i = B_q[\boldsymbol{u} \cos(\boldsymbol{q} \cdot \boldsymbol{r}_i) + \boldsymbol{v} \sin(\boldsymbol{q} \cdot \boldsymbol{r}_i)] \tag{5.58}$$

into eq. (5.46). We write the averaged spin as

$$\langle \boldsymbol{S}_i \rangle = m_q[\boldsymbol{u} \cos(\boldsymbol{q} \cdot \boldsymbol{r}_i) + \boldsymbol{v} \sin(\boldsymbol{q} \cdot \boldsymbol{r}_i)]. \tag{5.59}$$

Then along with molecular field procedure, the effective Hamiltonian at site i is given by

$$\mathscr{H}_{\text{eff}}(i) = -(2m_q J_q + \mu B_q)[\boldsymbol{u} \cos(\boldsymbol{q} \cdot \boldsymbol{r}_i) + \boldsymbol{v} \sin(\boldsymbol{q} \cdot \boldsymbol{r}_i)] \cdot \boldsymbol{S}_i. \tag{5.60}$$

Then as is the course, a self-consistent equation is given by

$$m_q = S\mathcal{B}_S \left[\frac{S}{k_{\mathrm{B}}T} (2m_q J_q + \mu B_q) \right]. \tag{5.61}$$

This has a just same form as that in the ferromagnetism. If we define "helical magnetization" as μm_q, we obtain the helical magnetization in paramagnetic states as

$$\chi_q = \lim_{B_q \to 0} \frac{\mu m_q}{B_q} = \chi_0 \left(1 - \frac{2J_q}{\mu^2}\chi_0\right)^{-1}. \tag{5.62}$$

The critical temperature for the appearance of helical order $T_{\boldsymbol{Q}}$ is given by

$$k_{\mathrm{B}} T_{\boldsymbol{Q}} = \frac{2}{3} S(S+1) J_{\boldsymbol{Q}}. \tag{5.63}$$

5.7.3 Observation of helimagnetism, skyrmion excitations

In the above, a helimagnetism in a Heisenberg model is considered. In real materials, it is said that $NiBr_2$ or β-MnO_2 may have situations close to the model. There have been found many materials with helimagnetisms. Holmium (Ho) has a helimagnetism originated from the RKKY interaction. The Dyaloshinsky-Moriya (DM) interaction often causes helimagnetism.

Here I would like to introduce an experimental method called "Lorentz microscope" for observing real space image of magnetic structure, and observation of helimagnetism and related magnetic phenomena. One of the most powerful methods to observe spin configurations is the neutron diffraction. Actually one of the motivations for finding helimagnetism was an anomalous neutron spectrum of β-MnO_2, etc. Despite the powerfulness of neutron diffraction in detecting periodic structures, it has difficulties in catching local real space images. Lorentz transmission microscope is one of the methods to observe local images [*2].

Figure 5.5 shows the principle of Lorentz microscope, which utilizes the bending of electron beams by Lorentz force from the magnetic field in samples. Complete re-focusing of electrons, however, restore the bending resulting in no-

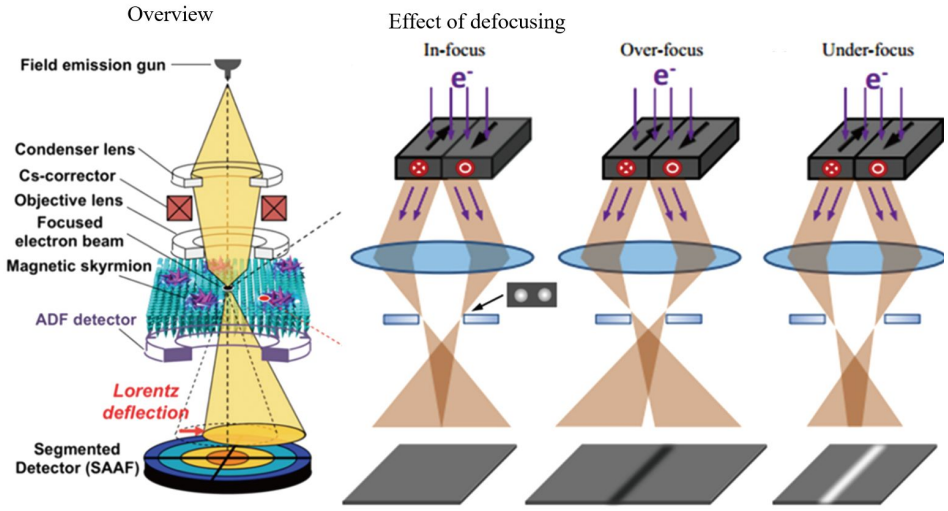

Fig. 5.5 Left panel: Illustration of electron beam lines in a Lorentz microscope. Focused electron beams go though a sample, and re-focused by electron lenses for forming an image on a screen. Three right panels: When the sample has inner magnetic field, the Lorentz force gives curving on the electron beams. Left in right: When the screen is just at the focal level, the bending are restored to have no contrast. Center in right: When the screen is a bit far, the over focusing results in a contrast. Right in right: When the screen is closer, the under focusing also results in a contrast. From Li-cong et al. Ch. Phys. B **27**, 066802 ('18).

[*2] There are many others like traditional observation of distribution of magnetic powders, micro MOKE with utilizing the Kerr rotation, magnetic force microscope, which detects magnetic field gradient, scanning SQUID, etc.

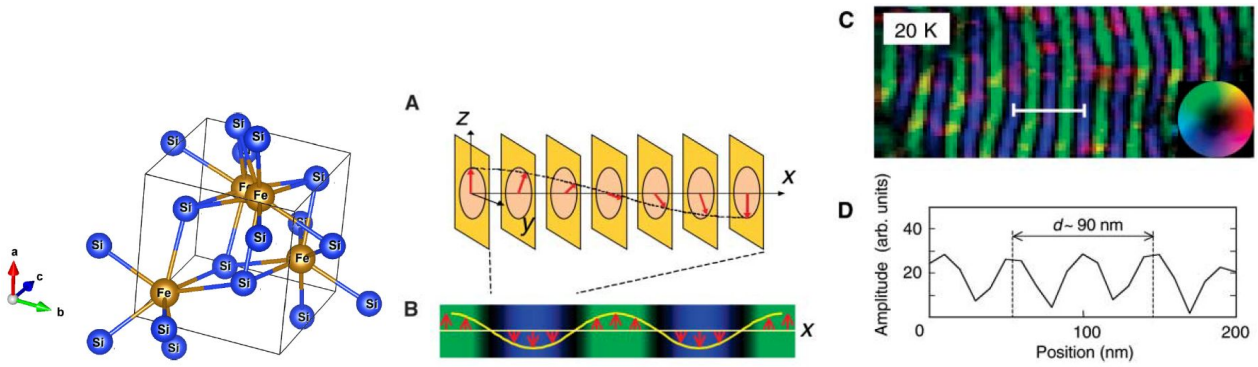

Fig. 5.6 Left: Cubic ϵ-FeSi (B20-type) structure without centrosymmetric point. A: Illustration of helimagnetism. B: Expected contrast in Lorentz micrograph for an observation in the angle of z-axis. C: False colored real space imaging of helimagnetism in $Fe_{1-x}Co_xSi$ at 20 K by a Lorentz microscope. D: Magnetic moment along z-axis deduced from the above[16].

contrast. Hence as illustrated in the right two panels in Fig. 5.5, the beams are a bit defocused to have a contrast, of which the intensity is reversed by the direction of defocusing.

Figure 5.6 shows an example of observing helimagnetism. The sample is $Fe_{1-x}Co_xSi$ in a non-centrosymmetric cubic ϵ-FeSi (B20) structure. Because of the lack of inversion symmetry, a term in similar form as an electric field appears in electric effective Hamiltonian and causes strong spin-orbit interaction. This leads to a strong DM interaction that creates the helimagnetism.

When one observes a helimagnetic spin ordered state in a side-view, as in Fig. 5.6A, B, the magnetization is modulated

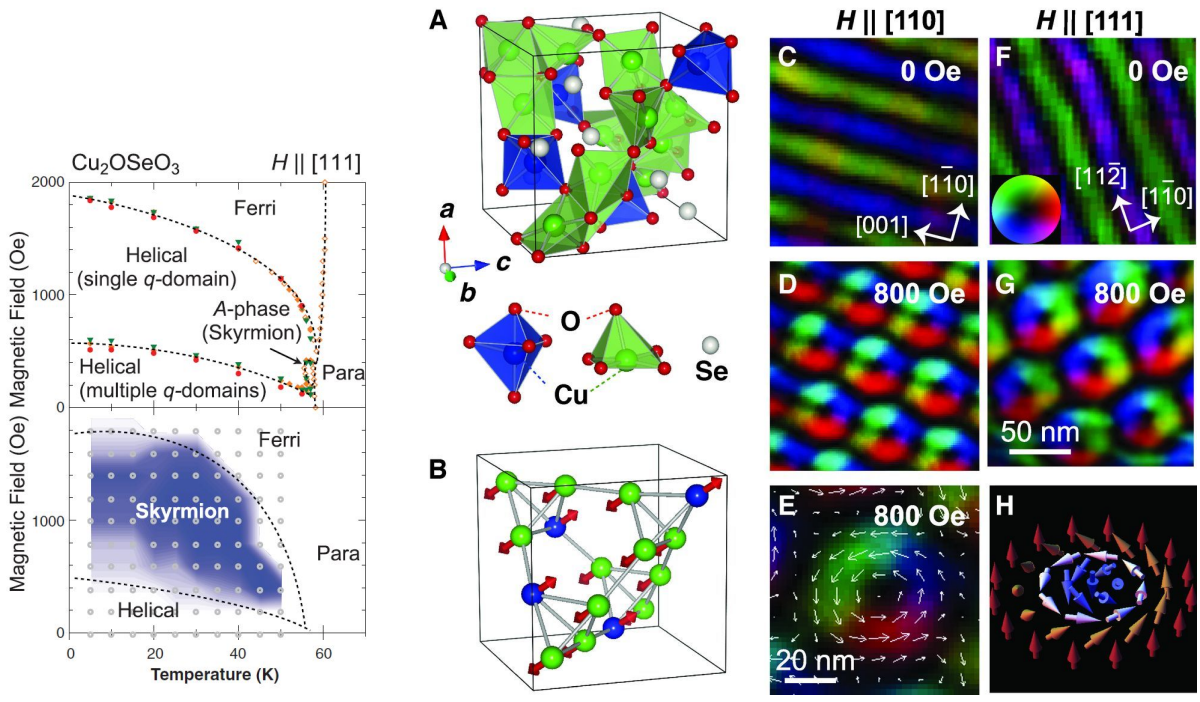

Fig. 5.7 Left: Experimentally obtained phase diagram of Cu_2OSeO_3. At low temperatures, low magnetic fields, it shows a helimagnetism, which is overtaken by a phase with skyrmion excitations with increasing the magnetic field. With further increase of the field, it changes to a ferrimagnetism. Right: A: Unit cell structure of Cu_2OSeO_3. B: Cu spin configuration in the ferrimagnetic phase. C $\sim$ G: Lorentz microscope images. At low magnetic field, a stripe due to helimagnetism, and at middle fields images of skyrmion are observed. H: shows schematic view of a skyrmion spin configuration. From ref. [17].

wavy in space. This corresponds to a Fresnel configuration of Lorentz microscope and actually in the image, a striping contrast is observed as in Fig. 5.6C.

Figure 5.7 shows skyrmion excitations observed with a Lorentz microscope. This is observed in Cu_2OSeO_3, which does not have inversion symmetry in lattice as shown in Fig. 5.7A, and the DM interaction causes a helimagnetism as in the phase diagram at low temperatures and at low magnetic fields. The helimagnetic phase is detected as stripe images by a Lorentz microscope as in C, F. With increasing the magnetic field, a phase with skyrmion excitation appears as in D, G, E. They are observed to be aligned periodically. Further increase in the field drives the system into a ferrimagnetic phase, of which spin configuration is shown in B.

5.8 Spin wave

The phase transitions with appearance of spontaneous magnetizations like ferromagnetic transition are an example of spontaneous symmetry breakings. They are also associated with the appearance of excited states called spin wave. Let us have a look on them.

5.8.1 Ferromagnetic spin wave

Here we need to consider dynamical properties of spins in ordered states. For that in ferromagnetic Heisenberg model (5.1), we consider the time evolution of operator $\boldsymbol{S}i$ by applying the Heisenberg equation of motion as

$$\hbar\frac{d\boldsymbol{S}_i}{dt} = \frac{1}{i}[\boldsymbol{S}_i, \mathscr{H}] = -2J\sum_{\delta}\boldsymbol{S}_{i+\delta}\times\boldsymbol{S}_i - \mu\boldsymbol{B}\times\boldsymbol{S}_i, \tag{5.64}$$

where δ is taken for the nearest neighbor of i. This calculation can be followed, with the use of commutation relation $[S^\alpha, S^\beta] = iS^\gamma$, $(\alpha,\beta,\gamma) = (x,y,z;$ cyclic), e.g., as

$$[S_i^x, S_i^xS_j^x + S_i^yS_j^y + S_i^zS_j^z] = [S_i^x, S_i^yS_j^y] + [S_i^x, S_i^zS_j^z] = i(S_i^zS_j^y - S_i^yS_j^z) = i(\boldsymbol{S}_j\times\boldsymbol{S}_i)_x.$$

Equation (5.64) is in the form of equation of motion for precession around the effective field (the external field plus the nearest neighbor interaction). Then we can foresee that the precessions are chained through the exchange interaction and forms a wave propagates over the spins. To see that we need to consider higher order approximation than the "averaged" field.

Then we consider the Fourier transform

$$\boldsymbol{S}_{\boldsymbol{q}} = \frac{1}{\sqrt{N}}\sum_i \boldsymbol{S}_i\exp(-i\boldsymbol{q}\cdot\boldsymbol{r}_i), \quad J_{\boldsymbol{q}} = \sum_{\delta} J\exp[-i\boldsymbol{q}\cdot(\boldsymbol{r}_i - \boldsymbol{r}_{i+\delta})], \tag{5.65}$$

and with substituting the inverse Fourier transformation into eq. (5.64), we represent (5.64) in the Fourier transformation as

$$\hbar\frac{d\boldsymbol{S}_{\boldsymbol{q}}}{dt} = -\frac{2}{\sqrt{N}}\sum_{\boldsymbol{q}'} J_{\boldsymbol{q}'}\boldsymbol{S}_{\boldsymbol{q}'}\times\boldsymbol{S}_{\boldsymbol{q}-\boldsymbol{q}'} - \mu\boldsymbol{B}\times\boldsymbol{S}_{\boldsymbol{q}}. \tag{5.66}$$

With the above, we extract a wave from the precessions of spins. By taking z-axis along magnetic field $\boldsymbol{B}$, $\langle\boldsymbol{S}_{\boldsymbol{0}}\rangle = \sqrt{N}S\boldsymbol{e}_z$ has by far the largest expectation value in a ferromagnetic state. Hence in the first term of rhs of (5.66), we ignore the terms other than $\langle\boldsymbol{S}_{\boldsymbol{0}}\rangle$ to obtain

$$\hbar\frac{d\boldsymbol{S}_{\boldsymbol{q}}}{dt} = -[2(J_{\boldsymbol{0}} - J_{\boldsymbol{q}})S + \mu B]\boldsymbol{e}_z\times\boldsymbol{S}_{\boldsymbol{q}}. \tag{5.67}$$

In each component

$$\left\{\begin{array}{l} \hbar\dfrac{dS_{\boldsymbol{q}x}}{dt} = \quad [2(J_{\boldsymbol{0}} - J_{\boldsymbol{q}})S + \mu B]S_{\boldsymbol{q}y}, \\ \hbar\dfrac{dS_{\boldsymbol{q}y}}{dt} = -[2(J_{\boldsymbol{0}} - J_{\boldsymbol{q}})S + \mu B]S_{\boldsymbol{q}x}, \\ \hbar\dfrac{dS_{\boldsymbol{q}z}}{dt} = 0. \end{array}\right. \tag{5.68}$$

For $S_{\boldsymbol{q}x}$ and $S_{\boldsymbol{q}y}$ these are harmonic oscillator equations. By comparison of this with

$$S_{\boldsymbol{q}x} + iS_{\boldsymbol{q}y} \propto \exp[-i\epsilon_{\boldsymbol{q}}t/\hbar], \tag{5.69}$$

we obtain the energy $\epsilon_{\boldsymbol{q}}$ of precession in $\boldsymbol{q}$ space as

$$\epsilon_{\boldsymbol{q}} = 2(J_{\boldsymbol{0}} - J_{\boldsymbol{q}})S + \mu B. \tag{5.70}$$

Because the precession is in $\boldsymbol{q}$-space, this represents a propagating wave in real space.

5.8.2 Holstein-Primakoff transformation

As is the case of Larmor precession, the equation of motion derived quantum mechanically has the same form as classical one. Then next we consider quantization of this wave. For a spin operator $\boldsymbol{S}$, we write an eigenfunction $|m\rangle$ of S_z with eigenvalue m ($m = -S, -S+1, \cdots, S-1, S$). The operation of up-down operators $S_\pm = S_x \pm S_y$ gives

$$\left.\begin{array}{l} S_+ |m\rangle = \sqrt{S(S+1) - m(m+1)}\, |m+1\rangle\,, \\ S_- |m\rangle = \sqrt{S(S+1) - m(m-1)}\, |m-1\rangle\,. \end{array}\right\} \tag{5.71}$$

Let us express a spin operator with creation and annihilation operators $a^\dagger$, a of bosons. For that we take the state $S_z = S$, i.e., $|S\rangle$ as the vacuum of boson, and $|S-n\rangle$ as n boson state. Namely,

$$a\,|S\rangle = 0, \quad |S-n\rangle = \frac{1}{\sqrt{n!}}(a^\dagger)^n\,|S\rangle\,. \tag{5.72}$$

Then with $\hat{n} = a^\dagger a$, we can formally write

$$\left.\begin{array}{l} S_z = S - \hat{n}, \\ S_+ = \sqrt{2S - \hat{n}}\; a, \\ S_- = a^\dagger\sqrt{2S - \hat{n}}. \end{array}\right\} \tag{5.73}$$

The above is called **Holstein-Primakoff transformation**.

Appendix 9A: Various “magnetism”

There are many ways to classify magnetisms and the classification itself is not very important. For example, as a macroscopic phenomena, there is “ferromagnetism”. However this contains a wide variety of magnetisms including “all-aligned” simple magnetism, ferrimagnetism, canted anti-ferromagnetism, etc. If we count for metastable configuration, the number of classes is huge, and the classification brings little knowledge. Here I would like to introduce some magnetisms to have smooth talks with experts on magnetism.

9A.1 Paramagnetism

So far we have seen the paramagnetism by local moments and that by itinerant electrons (Pauli paramagnetism). The Pauli paramagnetism usually have smaller contribution to the susceptibility and for the detection, a combination with other methods is usually required.

There are the cases that a finite number of spins form an ordered state, which does not spread over the system. Such a system generally shows paramagnetism with a huge magnetic moment, which is called **superparamagnetism**. The behavior of susceptibility resembles those of anti-ferromagnetism or spin-glass. Distinction of these is sometimes difficult.

9A.2 Diamagnetism

As we saw in the Landau diamagnetism in metals, usually diamagnetism originates from orbital motion of electrons. It sometimes becomes very large reflecting peculiar band structures as we saw in the section of graphite. Since water also has a large diamagnetism, various things including water cause magnetic levitation in a very large magnetic field. As a bit special example, the superconductors have perfect diamagnetism (the Meissner effect).

9A.3 Ferromagnetism

As mentioned at the beginning of this section, there can be various definitions of ”ferromagnetism.” It often refers to the case where itinerant electrons exist like metal and their spins become imbalanced to generate spontaneous magnetization. Also ferrimagnetism is often called ”ferromagnetism.”

9A.4 Anti-ferromagnetism

すでに見たように，磁気副格子内でスピンの向きが揃っているが，副格子のモーメントが互いに反転しているために全体としては自発磁化を持たないように見える (帯磁率が発散しない) ものを反強磁性と呼ぶ.

9A.5 Ferrimagnetism

As in anti-ferromagnets, neighboring moments have antiparallel alignment. However because there are unbalances in the size of moments or the numbers of magnetic sublattices, total spontaneous magnetization appears in ferrimagnetism. Oxide ferromagnets like ferrites, garnets are this type.

9A.6 Canted anti-ferromagnetism

This type also has anti-ferromagnetic interactions though the moments in magnetic sublattices are not completely inverted, but canted. Some of ferrite. Total spontaneous magnetization is generally small (weak ferromagnetism).

9A.7 Helimagnetism

The magnetic moments are arranged helically in space, and total spontaneous magnetization vanishes. On the other hand, ”chirality” occurs depending on the winding direction of the spiral, which causes various phenomena. In some cases, a topological excitation called “skyrmion” appears, and they form a lattice. This kinds of materials have been attracting attentions in these decades.

9A.8 Spin density wave

The state in which the spin density and direction are spatially distributed in a wavy manner is called the spin density wave (SDW). There are also anti-ferromagnetic SDW without total magnetization, and ferrimagnetic SDW with a total magnetization.

9A.9 Spin glass

When the localized magnetic moments exist randomly in space and the interaction between the moments is also random, the angles of the moments are randomly frozen, as in a glass state (amorphous state) in which atoms are randomly aggregated. This is called spin glass. It is found in dilute magnetic alloys containing magnetic atoms as impurities. In ferromagnetism and anti-ferromagnetism, there are only a few stable states of free energy, but in spin glass, there are a large number of metastable points. The Nishimori quantum annealing theory is built on the mathematical similarity between the relaxation from such metastable points to the true ground state by quantum tunneling (annealing) and a kind of optimization problem. This is the basics of modern quantum annealing computation[18]. The behavior of the magnetism is similar to that of anti-ferromagnetic materials. When cooling in a magnetic field, the temperature dependence becomes weaker on the lower temperature side than the spin glass transition point, and in zero magnetic field cooling, the magnetism disappears near zero degrees. As the temperature rises, the magnetization also rises and joins the cooling value in the magnetic field at the transition point.

References

[1] D. C. Johnston. Magnetic susceptibility of collinear and noncollinear heisenberg antiferromagnets. *Phys. Rev. Lett.*, Vol. 109, p. 077201, Aug 2012.

[2] W. L. Roth. Magnetic structures of mno, feo, coo, and nio. *Phys. Rev.*, Vol. 110, pp. 1333–1341, Jun 1958.

[3] Sergio M. Rezende, Antonio Azevedo, and Roberto L. Rodríguez-Suárez. Introduction to antiferromagnetic magnons. *Journal of Applied Physics*, Vol. 126, No. 15, p. 151101, October 2019.

[4] Z. Yamani, Z. Tun, and D. H. Ryan. Neutron scattering study of the classical antiferromagnet MnF_2: a perfect hands-on neutron scattering teaching courseSpecial issue on neutron scattering in canada. *Canadian Journal of Physics*, Vol. 88, No. 10, pp. 771–797, October 2010.

[5] Dawid Pinkowicz, Michał Rams, Wojciech Nitek, Bernard Czarnecki, and Barbara Sieklucka. Evidence for magnetic anisotropy of [NbIV(CN)8]4- in a pillared-layered mn2nb framework showing spin-flop transition. *Chemical Communications*, Vol. 48, No. 67, p. 8323, 2012.

[6] Sanjib Banik, Kalipada Das, Tapas Paramanik, Niranjan Prasad Lalla, Biswarup Satpati, Kalpataru Pradhan, and Indranil Das. Huge magnetoresistance and ultrasharp metamagnetic transition in polycrystalline $sm_{0.5}ca_{0.25}sr_{0.25}mno_3$. *NPG Asia Materials*, Vol. 10, No. 9, pp. 923–930, September 2018.

[7] Noriki Terada and Hiroaki Mamiya. High-efficiency magnetic refrigeration using holmium. *Nature Communications*, Vol. 12, No. 1, February 2021.

[8] 近角聡信. 強磁性体の物理 (上): 物質の磁性 (物理学選書 4). 裳華房, 単行本, 10 1978.

[9] A Broese van Groenou, P.F Bongers, and A.L Stuyts. Magnetism, microstructure and crystal chemistry of spinel ferrites. *Materials Science and Engineering*, Vol. 3, No. 6, pp. 317–392, February 1969.

[10] Chemistry310 at Penn State University. Chemistry libretexts; 8.7: Spinel, perovskite, and rutile structures, 2021. https://chem.libretexts.org/Bookshelves/Inorganic_Chemistry/Book%3A_

Introduction_to_Inorganic_Chemistry_%28Wikibook%29/08%3A_Ionic_and_Covalent_Solids_-_Structures/8.07%3A_Spinel_Perovskite_and_Rutile_Structures also https://en.wikibooks.org/wiki/Introduction_to_Inorganic_Chemistry/Ionic_and_Covalent_Solids_-_Structures#_8.6_Spinel,_perovskite,_and_rutile_structures.

[11] 電気学会マグネティックス技術委員会（編）. 磁気工学の基礎と応用. コロナ社, 10 2013.

[12] Alex Goldman. *Modern Ferrite Technology*. Van Nostrand Reinhold, 12 1990.

[13] R. Hasegawa, B. E. Argyle, and L-J. Tao. Temperature dependence of magnetization in amorphous gd-co-mo films. In *AIP Conference Proceedings*, Vol. 24, p. 110. AIP, 1975.

[14] Rolf Stinshoff, Ajaya K. Nayak, Gerhard H. Fecher, Benjamin Balke, Siham Ouardi, Yurii Skourski, Tetsuya Nakamura, and Claudia Felser. Completely compensated ferrimagnetism and sublattice spin crossing in the half-metallic heusler compound $\mathrm{mn}_{1.5}\,\mathrm{fev}_{0.5}\,\mathrm{Al}$. *Phys. Rev. B*, Vol. 95, p. 060410, Feb 2017.

[15] Akio Yoshimori. A new type of antiferromagnetic structure in the rutile type crystal. *Journal of the Physical Society of Japan*, Vol. 14, No. 6, pp. 807–821, June 1959.

[16] Masaya Uchida, Yoshinori Onose, Yoshio Matsui, and Yoshinori Tokura. Real-space observation of helical spin order. *Science*, Vol. 311, No. 5759, pp. 359–361, January 2006.

[17] S. Seki, X. Z. Yu, S. Ishiwata, and Y. Tokura. Observation of skyrmions in a multiferroic material. *Science*, Vol. 336, No. 6078, pp. 198–201, April 2012.

[18] 西森秀稔, 大関真之. 量子アニーリングの基礎 (基本法則から読み解く物理学最前線 18). 共立出版, 5 2018.